Microelectronic Engineering 87 (2010) 566–572

Contents lists available at ScienceDirect

Microelectronic Engineering

journal homepage: www.elsevier.com/locate/mee

Kinetics of the ruthenium thin film deposition from supercritical carbon dioxide by the hydrogen reduction of $Ru(tmhd)_2cod$

Christos F. Karanikas [a], James J. Watkins [b,*]

[a] Department of Chemical Engineering, University of Massachusetts Amherst, Amherst, MA 01003, USA
[b] Department of Polymer Science and Engineering, University of Massachusetts Amherst, Amherst, MA 01003, USA

ARTICLE INFO

Article history:
Received 21 September 2008
Received in revised form 13 June 2009
Accepted 11 August 2009
Available online 19 August 2009

Keywords:
Kinetics
Thin film
Ruthenium
Supercritical fluid deposition

ABSTRACT

The kinetics of ruthenium thin film deposition via the hydrogen assisted reduction of bis(2,2,6,6-tetramethyl-3,5-heptanedionato)(1,5-cyclooctadiene)ruthenium(II) [$Ru(tmhd)_2cod$] in supercritical carbon dioxide was studied. Deposition temperature was varied from 240 °C to 280 °C and the apparent activation energy was determined to be 45.3 kJ/mol. Deposition rates up to 30 nm/min were attained. The growth rate dependence on precursor concentration between 0 and 0.2 wt.% in CO_2 was studied at 260 °C using excess hydrogen. The results indicated first order deposition kinetics with respect to precursor at concentrations lower than 0.06 wt.% and zero order dependence at concentrations above 0.06 wt.%. The ability to access regimes of zero order growth kinetics is advantageous for conformal depositions in high aspect ratio features. Growth rate was second order with respect to hydrogen at concentrations less than 0.26 wt.% and zero order at higher concentrations. The reaction byproducts, cyclooctadiene and cyclooctene, both had negative first order effects on growth rate while cyclooctane had a small negative impact on film growth rate. The effect of reaction pressure on the growth rate was studied at a constant reaction temperature of 260 °C and pressures between 159 bar and 200 bar and found to have no significant effect on the growth rate.

1. Introduction

The preparation of nanostructured elements for future generations of microelectronic and optoelectronic devices will require the deposition of high purity, conformal, metal thin films within narrow (<100 nm) and/or high aspect ratio (>10) features. For example, microprocessors are predicted to operate at the 45 nm node as early as 2010 [1]. Ruthenium's characteristic properties (ρ = 7.2 μΩ-cm at 25 °C, 6.5 on Moh's scale, T_m = 2427 °C and equivalent oxide thickness (EOT) of less than one) render Ru an attractive candidate for complementary metal-oxide semiconductor (CMOS) gates for dynamic (DRAM) and nonvolatile ferroelectric (FeRAM) random access memory electrodes [2,3]. Other applications include conductive diffusion barrier layers for copper interconnects in semiconductors.

Ruthenium has typically been deposited by physical vapor deposition (PVD), chemical vapor deposition (CVD) or atomic layer deposition (ALD) using a wide range or precursors [4–28]. Line of sight limitations for most PVD techniques present difficulties when conformal deposition within high aspect ratio features is needed. ALD yields excellent step coverage, but sub-monolayer deposition thickness per reaction cycle presents deposition rate challenges for films beyond a few nanometers in thickness. Ruthenium films deposited via CVD can contain high impurity levels due to ligand decomposition products. CVD environments are also typically oxidizing, which can lead to high levels of oxygen contamination in the film or in adjacent barrier layers such as Ta [29]. In addition, precursor conversion is typically less than 10% due to precursor vapor pressure limitations causing the CVD process to be mass transfer limited [30,31]. Thus the deposition of conformal films in high aspect ratio features via CVD remains a challenge.

Recently, we reported excellent step coverage for the deposition of conformal ruthenium films deposited within complex geometries using supercritical fluid deposition (SFD) under reducing conditions. In that study, the hydrogen assisted reduction organoruthenium complexes, including triruthenium dodecacarbonyl ($Ru_3(CO)_{12}$), tris(2,2,6,6-tetramethyl-heptane-3,5-dionato)ruthenium ($Ru(tmhd)_3$), and bis(2,2,6,6-tetramethyl heptane-3,5-dionato)(1,5-cyclooctadiene) ruthenium ($Ru(tmhd)_2cod$) yielded highly reflective thin films with resistivities as low as 22 μΩ cm for a 33 nm thick film and excellent step coverage of high purity films was achieved within 200 nm × 300 nm trenches on patterned tantalum-coated surfaces and within 2 μm × 30 μm and 300 nm × 1.2 μm via structures on etched silicon substrates [32] SFD is a hybrid approach to reactive metal deposition that combines the advantages of solution-based processes, namely high precursor concentration and the elimination of precursor volatility con-

* Corresponding author.
E-mail address: watkins@polysci.umass.edu (J.J. Watkins).

0167-9317/$ - see front matter © 2009 Elsevier B.V. All rights reserved.
doi:10.1016/j.mee.2009.08.011

straints, with those of vapor phase techniques, namely favorable transport properties and the absence of surface tension. High fluid phase precursor concentrations are important because they can yield conformal coverage if deposition kinetics can be shifted into a regime of surface reaction rate control. To date, a number of metal films have been deposited using SFD, which include Cu, Au, Ag, Pt, Pd, Ni, Rh, Ru, Co, Ir and alloys [32–46]. While the utility of SFD, especially for conformal films, is established, there are few kinetic studies of the process. Recently, Zong and Watkins, reported the kinetics and reaction mechanism of copper SFD via the hydrogen assisted reduction of bis(2,2,7-trimethyloctane-3,5-dionato)copper(II), Cu(tmod)$_2$, and proposed a Langmuir–Hinshelwood rate expression for the reaction [46]. This was the first time the kinetics of an SFD process was studied. Cu SFD using this precursor was found to be mechanistically similar to the CVD process and was modeled accordingly. However, Zong found that unlike in CVD, the high precursor concentration accessible in SFD yielded surface reaction rate limited, zero order deposition kinetics with respect to precursor over broad ranges of precursor concentrations. Here we present a comprehensive study of ruthenium SFD kinetics via the hydrogen assisted reduction of bis(2,2,6,6-tetramethyl-heptane-3,5-dionato)(1,5-cyclooctadiene)ruthenium(II), Ru(tmhd)$_2$cod and find similar results for access to zero order deposition rates at elevated precursor concentrations that are presumably surface reaction rate limited.

2. Results and discussion

2.1. Film quality

High quality ruthenium films were deposited in this study. The purity of films was determined using X-ray photoelectron spectroscopy (XPS). Fig. 1 (bottom right) shows an XPS sputter depth profile of an 83 nm thick ruthenium film deposited by the hydrogen assisted reduction of Ru(tmhd)$_2$cod from a 0.09 wt.% solution of precursor in CO_2 at a stage temperature of 260 °C in the presence of excess hydrogen. No significant contamination was observed throughout the bulk of the film. Although carbon concentration was not determined directly from the C1s peak due to overlapping of its orbital energy position with that of the Ru 3d orbital, it is possible to determine if carbon impurities are present. The peak separation between the Ru $3d_{3/2}$ and $3d_{5/2}$ peak is known to be 4.2 eV in pure Ruthenium [47–51]. Additionally, the peak height ratio is known to be approximately 1.5. Convolution of the Ru peaks with

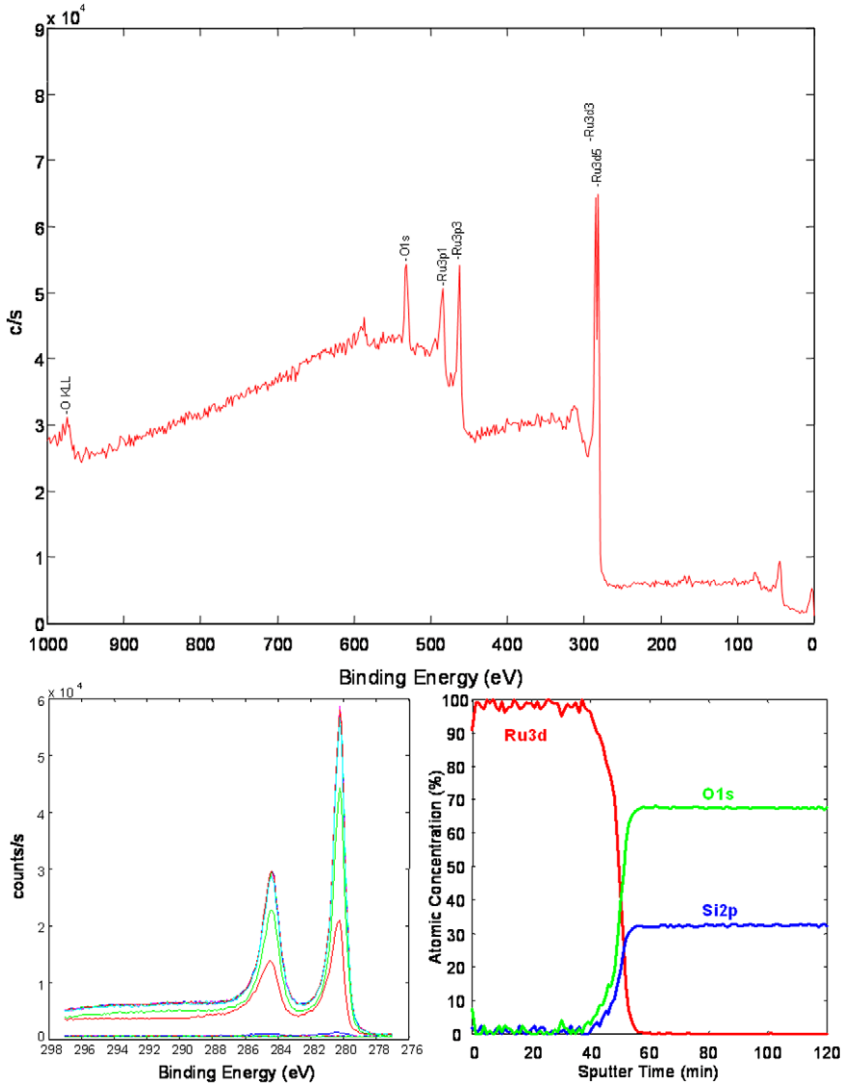

Fig. 1. X-ray photoelectron spectroscopy survey spectrum (top) of a Ru film deposited by SFD. The ruthenium 3d orbital binding energy region (bottom left) and sputter depth profile (bottom right) indicate a high purity film. Reaction conditions: 260 °C, 172 bar, 0.09 wt.% Ru(tmhd)$_2$cod, 0.3 wt.% hydrogen, 3 min heating.

the C1s peaks would be expected to alter these relationships. Fig. 1 (top) shows an XPS survey spectrum with enlarged (bottom left) Ru 3d binding energy fingerprint region. The observed results reflect these expectations indicating a high purity ruthenium film.

Resistivity measurements were consistent with high film purity. Sheet resistance was calculated from film resistivity and thickness measurements and was determined to be approximately 20 μΩ-cm. While the measured resistance is greater than that of bulk Ru (7.6 μΩ-cm), this is not unexpected due to the thin nature of the film and grain boundary effects. Had significant levels of carbon contamination been present, sheet resistance values would be expected to be much higher.

A cross sectional field emission scanning electron microscopy, FESEM, is shown in Fig. 2. The inset is a height image from atomic force microscopy, AFM, analysis. The SEM image indicates that continuous ruthenium films were deposited on the planar silicon substrates, while AFM data indicates a mean surface roughness of 1 nm. Examples of excellent step coverage in high aspect ratios using this deposition chemistry under similar conditions can be found in our earlier report [32].

2.2. Temperature dependence

The Arrhenius equation was used to determine the activation energy for the SFD of ruthenium films deposited by the hydrogen assisted reduction of $Ru(tmhd)_2cod$. The temperature dependence of growth rate was studied over the range of 240–280 °C in 10 °C steps (Fig. 3). The experiments were performed at a constant reaction pressure of 172 bar, a precursor concentration of 0.07 wt.% and hydrogen concentration of 0.3 wt.%. The apparent activation energy was found to be 45.3 kJ/mol. In other kinetic studies of interest, Papadatos et al., found the activation energy for $Ru(tmhd)_2cod$ deposition on SiO_2/Si to be 41.3 kJ/mol using a metal organic CVD (MOCVD) process between 400 and 450 °C, 1 torr and oxygen and hydrogen as the reactive gases and 59.4 kJ/mol for PACVD process using the same precursor [52]. In 2004, the same group also found the activation energy for bis(ethylcyclopentadienyl)ruthenium, $Ru(EtCp)_2$, on SiO_2/Si to be 43 kJ/mol using MOCVD between 320 and 360 °C, 0.3 torr and oxygen as the reactive gas [53]. In 2003, Dey et al., used a low pressure, horizontal MOCVD hot wall reactor to study the deposition of ruthenium from the oxygen-assisted pyrolysis of $Ru(tmhd)_2cod$ by liquid-source MOCVD [54]. The depositions were conducted on $HfO_2/SiO_2/Si$ substrates between temperatures of 250–320 °C. The activation energy was found to be 136 kJ/mol for the surface reaction limited regime, which occurred between 250 and 290 °C and below. As temperature increased past 290 °C, the surface reaction limited regime for growth gave way to the mass transfer limited regime as growth rate became independent of temperature.

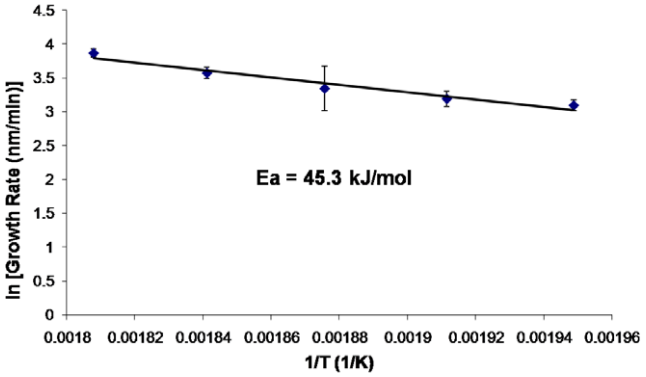

Fig. 3. Temperature dependence for hydrogen assisted Ru deposition from carbon dioxide. Reaction conditions: 240–280 °C in 10 °C steps, 172 bar, 0.07 wt.% $Ru(tmhd)_2cod$, 0.3 wt.% hydrogen, 3 min heating. The apparent activation energy is 45.3 kJ/mol.

2.3. Precursor concentration dependence

The growth rate dependence on precursor concentration was studied at a constant temperature of 260 °C and 280 °C (Fig. 4). The initial reaction pressure for all reactions was 172 bar. Hydro-

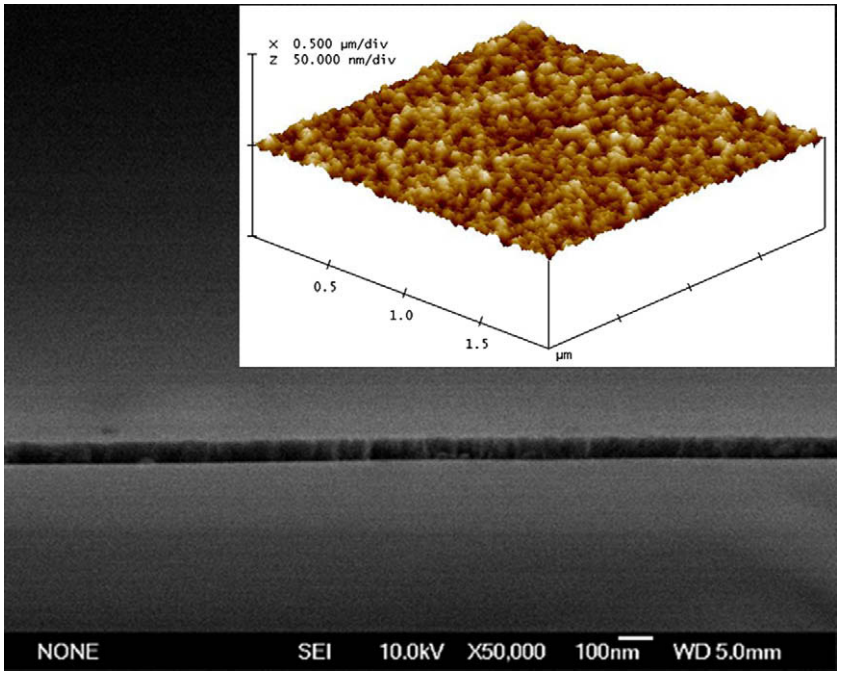

Fig. 2. Field emission scanning electron microscope cross section image of a conformal, 77 nm thick, ruthenium film deposited by SFD. The inset is an atomic force microscopy image of the film. The mean surface roughness is 1 nm. Reaction conditions: 260 °C, 145 bar, 0.09 wt.% $Ru(tmhd)_2cod$, 0.3 wt.% hydrogen, 3 min heating.

gen concentration was also held constant for all reactions at 0.3 wt.%. At low precursor concentrations, less than 0.06 wt.%, the growth rate dependence on precursor concentration was first order. Above precursor concentrations of 0.06 wt.%, there was no increase in the growth rate with concentration, indicating zero order dependence. The zero order kinetics of the growth rate with respect to precursor concentration is an enabling feature of SFD that yields conformal film deposition over a broad process window. The observed zero order kinetics suggests that the rate determining step for this deposition was either the surface reaction or the desorption of byproducts from the active catalytic surface sites.

2.4. Pressure dependence

Increasing pressure during SFD increases the density of supercritical carbon dioxide thereby improving its solvent strength. Increases in solvent strength in turn promotes desorption of the precursor decomposition products, which are soluble in the fluid. The effect of pressure (solvent density) on the growth rate may therefore provide insight into the rate-controlling step. If the desorption of precursor was promoted, more surface sites should become available.

The results of the study of pressure dependence are shown in Fig. 5. The temperature was held constant at 260 °C and the hydrogen concentration was held constant at 0.3 wt.% while the pressure was varied between 135 bar and 200 bar. For the entire range of pressures that was studied, it was found that the reaction pressure has no systematic effect on the growth rate of the ruthenium film. The growth rate remained constant at approximately 27 nm/min. This result suggested that over the range of solvent strengths accessible, density mediated enhancements in the desorption of precursor decomposition products from the active surface sites did not affect the rate of film growth.

2.5. Hydrogen concentration dependence

Hydrogen's effect on the growth rate of ruthenium films was studied. The data are shown in Fig. 6. The study was performed at a constant reaction temperature of 260 °C for 3 min, 172 bar and $Ru(tmhd)_2cod$ at a loading of 0.09 wt.%. At concentrations above 0.26 wt.% growth rate of the ruthenium film was independent of hydrogen concentration. It was noted that at hydrogen concentrations of 0.4 wt.% and above, the films delaminated, presumably due to increased stress in the film. At concentrations below 0.26 wt.%, the film growth rate increased with increasing

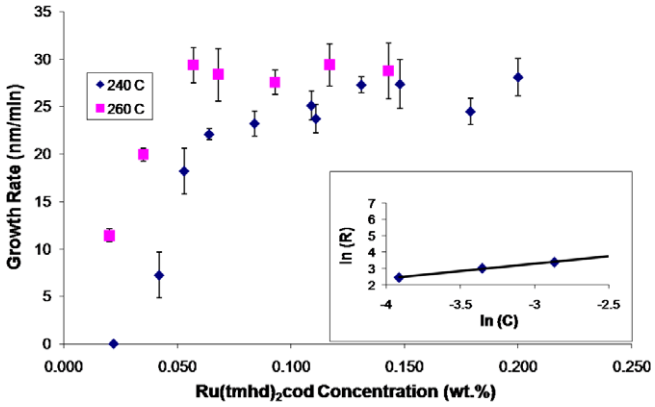

Fig. 4. Ru film deposition rate dependence on $Ru(tmhd)_2cod$ concentration. Reaction conditions: 260 °C and 280 °C, 172 bar, 0.3 wt.% hydrogen, 3 min heating. Zero order kinetics are observed at high precursor concentrations and first order kinetics are observed at lower precursor concentrations.

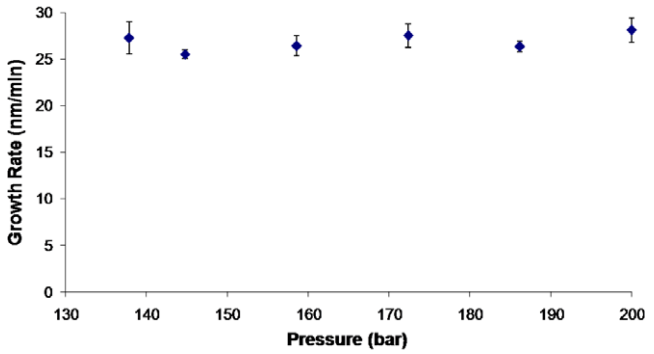

Fig. 5. Ru film deposition rate dependence on reaction pressure. Reaction conditions: 260 °C, 135–200 bar, 0.09 wt.% $Ru(tmhd)_2cod$, 0.3 wt.% hydrogen, 3 min heating. Pressure does not influence growth rate over the range of 135–200 bar.

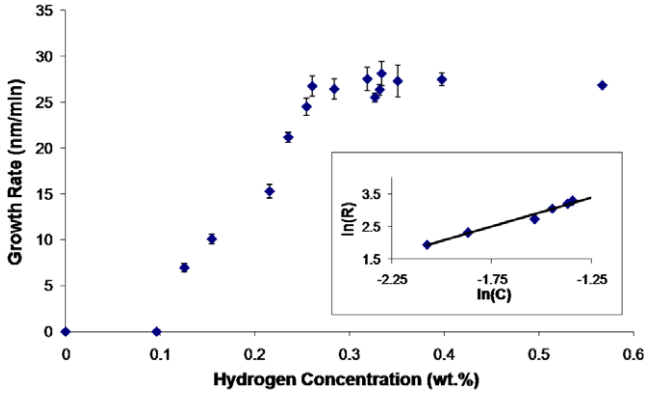

Fig. 6. Ru film deposition rate dependence on hydrogen concentration. Reaction conditions: 260 °C, 0.09 wt.% $Ru(tmhd)_2cod$, 0–0.6 wt.% hydrogen, 3 min heating. Using differential kinetics, zero order kinetics is observed at high hydrogen concentration and 2nd order kinetics at lower concentrations. Parasitic deposition is noted at 0.1 wt.% hydrogen and lower.

hydrogen concentration. The effect of hydrogen was 2nd order with respect to ruthenium film growth rate. At concentrations of 0.1 wt.% and below, there was no deposition, which was attributed to parasitic consumption of the hydrogen, possibly due to deposition on the exposed areas of the heated stage during the time that the substrate was reaching reactive conditions for film deposition.

2.6. Byproduct concentration dependence

The reaction decomposition products, 1,5-cyclooctadiene, cod, cyclooctane, cot, and 2,2,6,6-tetramethyl-heptane-3,5-dionato, tmhd, were studied to determine their effects on the growth rate. Each byproduct was tested independently of the others over specified ranges. The reactions were carried out at a constant reaction temperature of 260 °C for 3 min, 172 bar, 0.9 wt.% $Ru(tmhd)_2cod$, 0.3 wt.% hydrogen. Plots of the data are shown for tmhd, cod and cot in Figs. 7–9, respectively.

Tmhd and cod concentrations were varied from 0 wt.% to 0.9 wt.% and analysis of the data reveals a negative effect on the growth rate of the films. The differential method of rate analysis was used to determine the reaction order from the inset plot. The slope of the lines indicates that the growth rate has a negative ½ order dependence for each of the byproducts separately. There are two possibilities to account for this result. First, byproduct competition for hydrogen, due to hydrogenation, could consume the available hydrogen in the system. However, given that the amount of hydrogen in the reactor was in excess of 1000 times

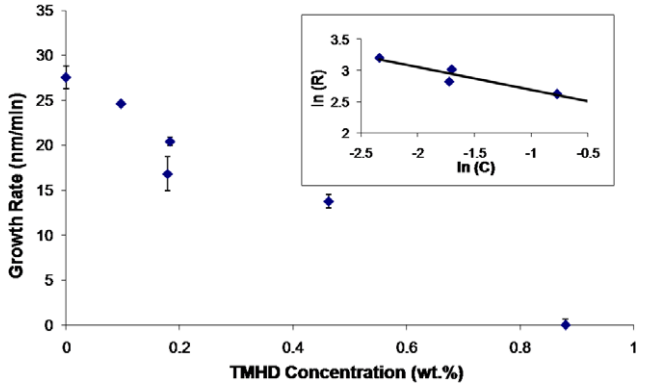

Fig. 7. Ru film deposition rate dependence on tmhd concentration. Reaction conditions: 260 °C, 0.09 wt.% Ru(tmhd)$_2$cod, 0.3 wt.% hydrogen, 3 min heating. Negative first order kinetics is observed with addition of tmhd from concentrations between 0 wt.% and 0.9 wt.%.

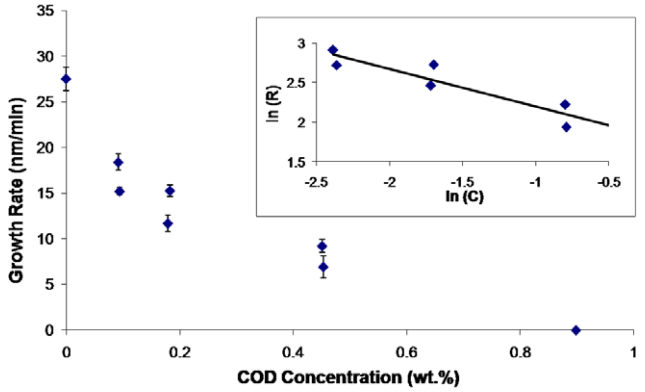

Fig. 8. Ru film deposition rate dependence on cod concentration. Reaction conditions: 260 °C, 0.09 wt.% Ru(tmhd)$_2$cod, 0.3 wt.% hydrogen, 3 min heating. Negative first order kinetics is observed with addition of cod from concentrations between 0 wt.% and 0.9 wt.%.

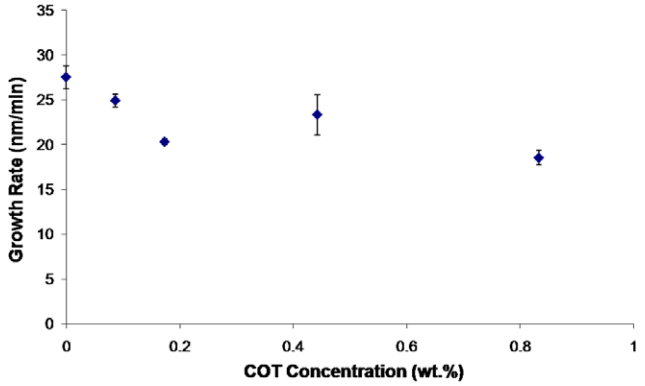

Fig. 9. Ru film deposition rate dependence on cot concentration. Reaction conditions: 260 °C, 0.09 wt.% Ru(tmhd)$_2$cod, 0.3 wt.% hydrogen, 3 min heating. Cot has a weak negative effect on growth rates between 0 wt.% and 0.9 wt.%.

the necessary amount for complete reduction of all loaded precursor, this is not likely the reason. A second and more likely possibility is that the unsaturated ligand decomposition products compete with the precursor for surface active sites thereby reducing the probability for a successful precursor adsorption and surface reaction.

Cot concentration was varied from 0 wt.% to 0.8 wt.%. The data indicate a slightly negative trend, but the effect is small if not within the error of the measurements. The approximate zero order dependence on cot concentration is likely attributed to the low affinity of absorption of the saturated cycloalkane relative to the other species in the system. During the deposition reaction, cot is formed via hydrogenation of cod and cyclooctene, coe.

2.7. Reaction orders and mechanism

In a previous report, Zong and Watkins [46] studied the hydrogen assisted reduction of bis(2,2,7-trimethyloctane-3,5-dionato)copper(II) in supercritical carbon dioxide via the use of a temperature controlled cold wall reactor with resistive substrate heating. The mechanism for reactive deposition via SFD was found to be similar to that of CVD. Specifically, the activation energy for Cu deposition from CO_2 was found to be 51.9 kJ/mol and a Langmuir–Hinshelwood rate expression was used to represent the data. It was found that growth rate was zero order with respect to pressure, precursor concentration and hydrogen concentration. However, at low concentrations of either precursor or hydrogen, half order dependence was noted. All byproducts studied indicated a negative effect on growth rate as concentration was increased. The rate determining step was the surface reaction.

The deposition of ruthenium from Ru(tmhd)$_2$cod, although similar in some respects to the deposition of copper from Cu(tmod)$_2$, is more complicated mechanistically due to the presence of the cyclooctadiene ligand and its subsequent hydrogenation products. Cod has been shown to enhance solubility of precursors in $SCCO_2$ because it can shield the positive electrical charge of various metal centers [55]. However, as the reaction proceeds and the unbound cod concentration increases, it competes for hydrogen in order to reduce to its monoene and also competes for surface active sites, thereby reducing the number of available sites for precursor adsorption.

A number of studies have been carried out in order to better understand the hydrogenation of cod. It was observed that 1,5 cod is isomerized to the conjugated diene, 1,3 cod, due to the lower energy state [56]. The conjugated diene then more quickly hydrogenated to coe. Additionally, the presence of cod and its ability to more readily adsorb to the surface hinders the adsorption and hydrogenation of coe to cot. It was found that the activation energy for the reduction of cod to coe over a Pd/α-Al_2O_3 catalyst was 74 kJ/mol while the activation energy was 98 kJ/mol for coe to cot [57]. Haas and Gaube [58] reported that the hydrogenation of cod occurs 6 times faster than the hydrogenation of coe. These findings indicated a first order hydrogenation with respect to cod at low concentrations and a much lower rate at higher concentrations of cod due to the competition for surface sites, resulting in low hydrogen surface concentrations at higher cod concentrations.

Given the observed experimental results of this study, our prior SFD report [46] and literature on CVD kinetics [30,31,52,54], the following overall reaction for the deposition of ruthenium by hydrogen assisted reduction of Ru(tmhd)$_2$cod in $SCCO_2$ is proposed.

$$\mathrm{Ru(tmhd)_2cod} + 2\mathrm{H_2} \rightarrow \mathrm{Ru_{(s)}} + \mathrm{coe_{(g)}} + 2\mathrm{(tmhd)H_{(g)}} \quad (1)$$

The conversion of cod to cot is not included in the proposed mechanism. We note that the film growth rate was found to be 2nd order with respect to hydrogen. We further note that previous studies indicate that the activation energy for conversion of coe to cot is higher than that for conversion of cod to coe [57]. The detailed mechanism supporting the proposed overall reaction is outlined in Eqs. (2)–(16).

$$\mathrm{Ru(tmhd)_2cod} + 2^* \leftrightarrow \mathrm{Ru\ tmhd\ cod^*} + \mathrm{tmhd^*} \quad (2)$$

$$\mathrm{Ru\ tmhd\ cod^{*}} + {}^{*} \leftrightarrow \mathrm{Ru\ cod^{*}} + \mathrm{tmhd^{*}} \quad (3)$$

$$\mathrm{Ru\ tmhd\ cod^{*}} + {}^{*} \leftrightarrow \mathrm{Ru\ tmhd^{*}} + \mathrm{cod^{*}} \quad (4)$$

$$\mathrm{Ru(tmhd)_2cod} + 2^{*} \leftrightarrow \mathrm{Ru(tmhd)_2^{*}} + \mathrm{cod^{*}} \quad (5)$$

$$\mathrm{Ru(tmhd)_2^{*}} + {}^{*} \leftrightarrow \mathrm{Ru\ tmhd^{*}} + \mathrm{tmhd^{*}} \quad (6)$$

$$\mathrm{H_2} + 2^{**} \leftrightarrow 2\mathrm{H^{**}} \quad (7)$$

$$2\mathrm{H^{**}} + \mathrm{cod^{*}} \leftrightarrow \mathrm{coe^{*}} + 2^{**} \quad (8)$$

$$2\mathrm{H^{**}} + \mathrm{coe^{*}} \leftrightarrow \mathrm{cot^{*}} + 2^{**} \quad (9)$$

$$\mathrm{cod^{*}} \leftrightarrow {}^{*} + \mathrm{cod_{(g)}} \quad (10)$$

$$\mathrm{coe^{*}} \leftrightarrow {}^{*} + \mathrm{coe_{(g)}} \quad (11)$$

$$\mathrm{cot^{*}} \leftrightarrow {}^{a}st + \mathrm{cot_{(g)}} \quad (12)$$

$$\mathrm{Ru\ tmhd^{*}} \leftrightarrow \mathrm{Ru_{(s)}} + \mathrm{tmhd^{*}} \quad (13)$$

$$\mathrm{Ru\ cod^{*}} \leftrightarrow \mathrm{Ru_{(s)}} + \mathrm{cod^{*}} \quad (14)$$

$$\mathrm{H^{**}} + \mathrm{tmhd^{*}} \rightarrow \mathrm{(tmhd)H^{*}} + {}^{**} \quad (15)$$

$$\mathrm{(tmhd)H^{*}} \leftrightarrow {}^{*} + \mathrm{(tmhd)H_{(g)}} \quad (16)$$

* and ** represent different surface active sites available for chemisorptions.

Eqs. (2)–(6) are the precursor adsorption to the first surface active site and ligand dissociation from the chelated metal center to the surface. Eq. (7) is the adsorption and dissociation of atomic hydrogen to molecular hydrogen on the second surface active site. Eqs. (8)–(12) are the conversion of cod to cot and their subsequent surface desorption equilibriums. Eqs. (13) and (14) are film formation steps. Eq. (15) is the probable rate determining step in which adsorbed hydrogen protonates bound ligand. Eq. (16) is the desorption of hydrogenated ligand back into the $SCCO_2$.

3. Conclusions

The kinetics of ruthenium film deposition by supercritical fluid deposition using bis(2,2,6,6-tetramethyl-heptane-3,5-dionato)(1,5-cyclooctadiene)ruthenium(II) as the precursor was studied. Reaction rate orders were determined as well as proposing a deposition mechanism. It was found that the apparent activation energy was 45.3 kJ/mol over the temperature range of 240–280 °C. The dependence of precursor concentration on growth rate was found to be first order for concentrations less than 0.06 wt.% and zero order for concentrations higher than 0.06 wt.%. Zero order deposition kinetics was an enabling feature of SFD that provides conformal film deposition in high aspect ratio and topographically complex features. It was also determined that reaction pressure has no effect on the growth rate over a large process window of 135–200 bar. Hydrogen concentration was studied and found to have a 2nd order effect on growth rate for concentrations less than 0.26 wt.% and a zero order effect on concentrations above that. Precursor decomposition products (tmhd, cod and cot) were studied. Tmhd and cod were shown to have a negative 1st order effect on film growth, which was attributed to their competition for surface active sites thereby decreasing the probability of a successful surface reaction. Cot showed negligible negative effects on growth rate, which was attributed to cot having no affinity for the surface. The surface reaction was found to be rate determining.

4. Experimental method and materials

Bis(2,2,6,6-tetramethyl-3,5-heptanedionato)(1,5-cyclooctadiene) ruthenium(II), 99%, (99.9% Ru), $Ru(tmhd)_2cod$, Fig. 10, was obtained from Strem Chemicals, Inc. (Newburyport, MA) and was ground using a mortar and pestle and used without any further purification. Approximately 98% pure *n*-heptane (Fisher Scientific, Pittsburgh, PA) was used as received without any further purification. Coleman grade (99.99%) carbon dioxide, ultra high purity (99.999%) hydrogen and prepurified grade (99.998%) nitrogen were used as received (Merriam Graves Corp, Charlestown, NH). A buna-N o-ring, size 2-236, was used for the high pressure and high temperature reactor seal (Marco Rubber and Plastic Products, Inc., North Andover, MA). Films were deposited on silicon (crystal orientation <100>, 500 nm thermally grown oxide, 1–100 micro-ohm centimeter, 750 micron total thickness) (Novellus, San Jose, CA).

The kinetics study was performed in a differential kinetics cold wall batch reactor comprised of two opposed 316 stainless steel flanges sealed with a 2-236 buna-N o-ring (Marco Rubber and Plastic Products, Inc., North Andover, MA). A cylindrical (r = 10 mm) aluminum stage heated by three 1″ long, 120 V, 100 W cartridge heaters (Omega Engineering, Inc., Stamford, CT) was used to quickly attain the desired reaction temperature. The wall of the stainless steel reactor is heated using four 3″ long, 120 V, 170 W cartridge heaters and was maintained at a lower temperature than the reaction stage in order to induce selective deposition to the higher temperature sample stage. The reaction was performed in a batch process and precursor conversion never exceeded 15% conversion, which allows for use of the differential method of rate analysis for the kinetics study.

For a typical reaction, a 12 mm by 12 mm silicon <100> wafer, with a 500 nm thermally grown oxide layer, was mounted to the aluminum heated stage and secured with two clips. A known amount of precursor was loaded into the vessel. The vessel was then sealed and placed behind protective polycarbonate housing. Then, using a constant flow of nitrogen, the reaction vessel was purged continuously over a 15 min period. The reactor wall was then heated to the desired temperature and allowed to equilibrate (t = 60 min). Carbon dioxide was introduced into the reactor using a computer-controlled syringe pump (Teledyne Isco, Inc., Lincoln, NE), which enabled precise volume measurement of the added CO_2. A suitable amount of time was allowed for complete dissolution of precursor [55] (t = 60 min) in the convection dominated flow [59] of the supercritical CO_2 in the reactor. For byproduct dependence reactions, the byproduct was loaded into an HPLC sample loop and then a known volume of byproduct was injected

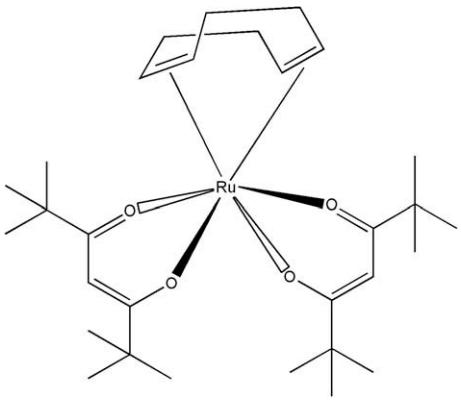

Fig. 10. Ruthenium precursor, bis(2,2,6,6-tetramethyl-heptane-3,5-dionato)(1,5-cyclooctadiene)ruthenium(II), $Ru(tmhd)_2cod$, used for supercritical fluid deposition kinetics study.

into the reactor. Next, hydrogen was loaded into the system using a manifold of known volume (70 mL). The moles of hydrogen injected were then calculated by pressure drop using the ideal gas law. The aluminum stage was then quickly heated (~15 s) to the desired reaction temperature and maintained for 3 min. The heated stage was then allowed to cool down (~15 s) while fresh CO_2 is used to flush multiple reactor volumes through the system to remove reaction byproducts and unreacted precursor. The effluent was passed through an activated carbon bed and silicon oil bubbler before being vented to the atmosphere. During the reaction, small gas phase samples of known volume were collected using HPLC sample loops. Samples were decompressed and the precursor was recovered in a known volume of *n*-heptane and the resulting solutions were analyzed using UV–visible spectroscopy in order to determine precursor concentrations in the fluid phase and confirm conversions of less than 15%. A differential method of rate analysis was used to analyze the data and propose a reaction mechanism as well as discover the reaction rate orders for the growth rate. The method of excess was used to account for multiple reactants.

The deposited films were characterized in order to obtain their thickness, purity, sheet resistance and roughness. Thickness measurements were performed using a Sloan Dektak^3 Surface Profiler. Growth rates were then calculated by dividing film thickness by reaction time. Film purity was determined by X-ray photoelectron spectroscopy (XPS) using a Quantum 2000 Scanning ESCA Microprobe (Physical Electronics USA, Chanhassen, MN) equipped with a monochromatic Al Kα X-ray source (1486.6 eV) and an Ar^+ ion-sputtering gun. Instrument settings were 15 kV and 25 W with 100 μm beam size. The take off angle was 45° and the ion-sputtering gun settings are 500 V, 700 nA, using a 0.5 mm × 0.5 mm square crater. Raw data was analyzed using Multipak, version 6.1A (Physical Electronics USA, Chanhassen, MN). The film's sheet resistance was measured with a four-point probe (Jandel Engineering Limited, Linslade, UK) and Keithley 2000 multimeter (Keithley Instruments, Inc., Cleveland, OH). Atomic force microscopy, AFM, is carried out using a Dimension 3100 atomic force microscope (Digital Instruments, a subsidiary of Veeco Instruments, Inc.). The AFM is interfaced with a NanoScope IIIa controller. Both tapping and contact modes are used. The software used is NanoScope (R) IIIa, version 5.12r3. The tips used for the microscope are Veeco, model RTESPW, 1–10 Ω-cm N doped Si. Tip specifications: T = 3.5–4.5 μm, L = 115–135 μm, W = 30–40 μm, f° = 312–342 kHz and k = 20–80 N/m.

Acknowledgements

Funding from NSF GOALI CTS – 0245002, NSF Center for Hierarchical Manufacturing NSEC (CMMI – 0531171) and NSF IGERT (DGE 0523634) is gratefully acknowledged. Facilities supported by the NSF Materials Research Science and Engineering Center (MRSEC) on Polymers and the NSF Center for Hierarchical Manufacturing (CMMI – 0531171) at the University of Massachusetts Amherst were used in this study.

References

[1] International Technology Roadmap for Semiconductors, http://www.itrs.net/, 2005.
[2] R. Chan, T.N. Arunagiri, Y. Zhang, O. Chyan, R.M. Wallace, M.J. Kim, T.Q. Hurd, Electrochemical and Solid-State Letters 7 (2004) G154–G157.
[3] C. Cheng, T. Arunagiri, O. Chyan, American Journal of Undergraduate Research 2 (2003) 11–18.
[4] T. Aoyama, K. Eguchi, Japanese Journal of Applied Physics 38 (1999) L1134–L1136.
[5] T. Aoyama, M. Kiyotoshi, S. Yamazaki, K. Eguchi, Japanese Journal of Applied Physics 38 (1999) 2194–2199.
[6] A.D. Berry, D.K. Brown, R. Kaplan, E.J. Cukauskas, Journal of Vacuum Science and Technology A: Vacuum, Surfaces, and Films 4 (1986) 215–218.
[7] E.P. Boyd, D.R. Ketchum, B. Deng, S.G. Shore, Chemistry of Materials 9 (1997) 1154–1158.
[8] Y. Chi, F.J. Lee, C.-S. Liu, USA Patent U.S. Patent 6,303,809, 2001.
[9] J.N. Crosby, R.S. Hanley, United States Patent U.S. Patent 4,250,210, 1981.
[10] X. Jin, C.P. Wade, X. Tao, E. Pao, Y. Wang, J. Zhao, USA Patent U.S. Patent 6,479,100, 2002.
[11] M. Kadoshima, T. Nabatame, M. Hiratani, Y. Nakamura, Japanese Journal of Applied Physics 41 (2002) L347–L350.
[12] J.J. Kim, D.H. Jung, M.S. Kim, S.H. Kim, D.Y. Yoon, Thin Solid Films 409 (2002) 28–32.
[13] Y.-H. Lai, Y.-L. Chen, Y. Chi, C.-S. Liu, A.J. Carty, S.-M. Peng, G.-H. Lee, Journal of Materials Chemistry 13 (2003) 1999–2006.
[14] M. Lashdaf, T. Hatanpaa, A.O.I. Krause, J. Lahtinen, M. Lindblad, M. Tiitta, Applied Catalysis A: General 241 (2003) 51–63.
[15] D.-J. Lee, S.-W. Kang, S.-W. Rhee, Thin Solid Films 413 (2002) 237–242.
[16] F.-J. Lee, Y. Chi, C.-S. Liu, P.-F. Hsu, T.-Y. Chou, S.-M. Peng, G.-H. Lee, Chemical Vapor Deposition 7 (2001) 99–101.
[17] J.-H. Lee, J.-Y. Kim, S.-W. Rhee, D. Yang, D.-H. Kim, C.-H. Yang, Y.-K. Han, C.-J. Hwang, Journal of Vacuum Science and Technology A: Vacuum, Surfaces, and Films 18 (2000) 2400–2403.
[18] J.M. Lee, J.C. Shin, C.S. Hwang, H.J. Kim, Journal of Vacuum Science and Technology A: Vacuum Surfaces, and Films 16 (1998) 2768–2771.
[19] S.-H. Lee, J.-K. Chun, J.-J. Hur, J.-S. Lee, G.-H. Rue, Y.-H. Bae, S.-H. Hahm, Y.-H. Lee, H.-H. Lee, IEEE Electron Device Letters 21 (2000) 261–263.
[20] Y. Matsui, M. Hiratani, T. Nabatame, Y. Shimamoto, S. Kimura, Electrochemical and Solid-State Letters 4 (2001) C9–C12.
[21] Y. Matsui, M. Hiratani, T. Nabatame, Y. Shimamoto, S. Kimura, Electrochemical and Solid-State Letters 5 (2002) C18–C21.
[22] T. Nabatame, M. Hiratani, M. Kadoshima, Y. Shimamoto, Japanese Journal of Applied Physics 39 (2000) L1188–L1190.
[23] S.-E. Park, H.-M. Kim, K.-B. Kim, S.-H. Min, Journal of the Electrochemical Society 147 (2000) 203–209.
[24] Y. Senzaki, Y. Senzaki, Y. Senzaki, Chemistry of Materials 5 (1993) 1715–1721.
[25] Y. Senzaki, F.B. McCormick, W.L. Gladfelter, Chemistry of Materials 4 (1992) 747–749.
[26] D.E. Trent, B. Paris, H.H. Krause, Inorganic Chemistry 3 (1964) 1057–1058.
[27] C.P. Wade, E. Pao, Y. Wang, J. Zhao, USA Patent 6,440,495, 2002.
[28] Q. Wang, J.G. Ekerdt, D. Gay, Y.-M. Sun, J.M. White, Applied Physics Letters 84 (2004) 1380–1382.
[29] L. Chen, N. Magtoto, B. Ekstrom, J. Kelber, Thin Solid Films 376 (2000) 115–123.
[30] M.J. Hampden-Smith, T.T. Kodas, Chemical Vapor Deposition 1 (1995) 8–23.
[31] M.J. Hampden-Smith, T.T. Kodas, Chemical Vapor Deposition 1 (1995) 39–48.
[32] A. O'Neil, J.J. Watkins, Chemistry of Materials 18 (2006) 5652–5658.
[33] J.M. Blackburn, A. Cabanas, D.P. Long, J.J. Watkins, Abstracts of Papers of the American Chemical Society 223 (2002) U663–U664.
[34] J.M. Blackburn, D.P. Long, A. Cabanas, J.J. Watkins, Science 294 (2001) 141–145.
[35] J.M. Blackburn, D.P. Long, J.J. Watkins, Chemistry of Materials 12 (2000) 2625–2631.
[36] A. Cabanas, J.M. Blackburn, J.J. Watkins, Microelectronic Engineering 64 (2002) 53–61.
[37] A. Cabanas, P. Long, J.J. Watkins, Chemistry of Materials 16 (2004) 2028–2033.
[38] A. Cabanas, X. Shan, J.J. Watkins, Chemistry of Materials 15 (2003) 2910–2916.
[39] N.E. Fernandes, S.M. Fisher, J.C. Poshusta, D.G. Vlachos, M. Tsapatsis, J.J. Watkins, Chemistry of Materials 13 (2001) 2023–2031.
[40] E.T. Hunde, J.J. Watkins, Chemistry of Materials 16 (2004) 498–503.
[41] E. Kondoh, Japanese Journal of Applied Physics 43 (2004) 3928–3933.
[42] E. Kondoh, Japanese Journal of Applied Physics 44 (2005) 5799–5802.
[43] E. Kondoh, K. Shigama, Thin Solid Films 491 (2005) 228–234.
[44] D.P. Long, J.M. Blackburn, J.J. Watkins, Advanced Materials 12 (2000) 913–915.
[45] J.J. Watkins, J.M. Blackburn, T.J. McCarthy, Chemistry of Materials 11 (1999) 213–215.
[46] Y. Zong, J.J. Watkins, Chemistry of Materials 17 (2005) 560–565.
[47] Y. Baer, P.F. Heden, J. Hedman, M. Klasson, C. Nordling, K. Siegbahn, Physica Scripta 1 (1970) 55–65.
[48] G.B. Fisher, N.E. Erikson, T.E. Madey, J. John, T. Yates, Surface Sciences 65 (1977) 210–228.
[49] B. Folkesson, Acta Chemica Scandinavica 27 (1973) 287–302.
[50] K.S. Kim, N. Winograd, Journal of Catalysis 35 (1974) 66–72.
[51] R. Nyholm, N. Martensson, Journal of Physics C: Solid State Physics 13 (1980) L279–L284.
[52] F. Papadatos, S. Skordas, Z. Patel, S. Consiglio, E. Eisenbraun, Material Research Society (2002).
[53] F. Papadatos, S. Consiglio, S. Skordas, E.T. Eisenbraun, A.E. Kaloyeros, J. Peck, D. Thompson, C. Hoover, Journal of Materials Research 19 (2004) 2947–2955.
[54] S.K. Dey, J. Goswami, A. Das, W. Cao, M. Floyd, R. Carpenter, Journal of Applied Physics 94 (2003) 774–777.
[55] O. Aschenbrenner, S. Kemper, N. Dahmena, K. Schaber, E. Dinjus, The Journal of Supercritical Fluids 41 (2007) 179–186.
[56] M. Di-Serio, V. Valato, A. Dimiccoli, L. Maffucci, P. Iengo, E. Santacesaria, Catalysis Today 66 (2001) 403–410.
[57] A. Schmidt, R. Schomacker, Industrial and Engineering Chemistry Research 46 (2007) 1677–1681.
[58] T. Haas, J. Gaube, Chemical Engineering and Technology 12 (1989) 45–53.
[59] X. Shan, D.P. Schmidt, J.J. Watkins, The Journal of Supercritical Fluids 40 (2007) 84–92.